
Approximate Inference Turns Deep Networks into Gaussian Processes

Mohammad Emtiyaz Khan
RIKEN Center for AI Project
Tokyo, Japan
emtiyaz.khan@riken.jp

Alexander Immer^{*†}
EPFL
Lausanne, Switzerland
alexander.immer@epfl.ch

Ehsan Abedi^{*†}
EPFL
Lausanne, Switzerland
ehsan.abedi@epfl.ch

Maciej Korzepa^{*†}
Technical University of Denmark
Kgs. Lyngby, Denmark
mjko@dtu.dk

Abstract

Deep neural networks (DNN) and Gaussian processes (GP) are two powerful models with several theoretical connections relating them, but the relationship between their training methods is not well understood. In this paper, we show that certain Gaussian posterior approximations for Bayesian DNNs are equivalent to GP posteriors. This enables us to relate solutions and iterations of a deep-learning algorithm to GP inference. As a result, we can obtain a GP kernel and a nonlinear feature map while training a DNN. Surprisingly, the resulting kernel is the neural tangent kernel. We show kernels obtained on real datasets and demonstrate the use of the GP marginal likelihood to tune hyperparameters of DNNs. Our work aims to facilitate further research on combining DNNs and GPs in practical settings.

1 Introduction

Deep neural networks (DNN) and Gaussian processes (GP) models are both powerful models with complementary strengths and weaknesses. DNNs achieve state-of-the-art results on many real-world problems providing scalable end-to-end learning, but they can overfit on small datasets and be overconfident. In contrast, GPs are suitable for small datasets and compute confidence estimates, but they are not scalable and choosing a good kernel in practice is challenging [3]. Combining their strengths to solve real-world problems is an important problem.

Theoretically, the two models are closely related to each other. Previous work has shown that as the width of a DNN increases to infinity, the DNN converges to a GP [4, 5, 13, 16, 22]. This relationship is surprising and gives us hope that a practical combination could be possible. Unfortunately, it is not clear how one can use such connections in practice, e.g., to perform fast inference in GPs by using training methods of DNNs, or to reduce overfitting in DNNs by using GP inference. We argue that, to solve such practical problems, we need the relationship not only between the models but also between their training procedures. The purpose of this paper is to provide such a theoretical relationship.

We present theoretical results aimed at connecting the training methods of deep learning and GP models. We show that the Gaussian posterior approximations for Bayesian DNNs, such as those obtained by Laplace approximation and variational inference (VI), are equivalent to posterior distributions of GP regression models. This result enables us to relate the solutions and iterations of a deep-learning algorithm to GP inference. See Fig. 1 for our approach called DNN2GP. In addition,

[†]Equal contribution. ^{*}This work is performed during an internship at the RIKEN Center for AI project.

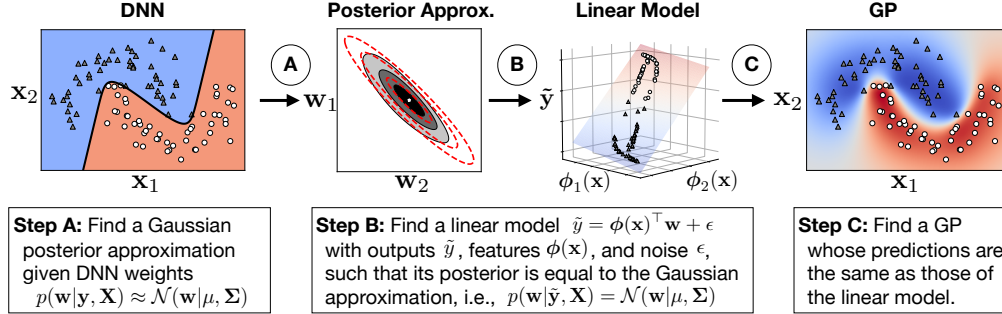


Figure 1: A summary of our approach called DNN2GP in three steps.

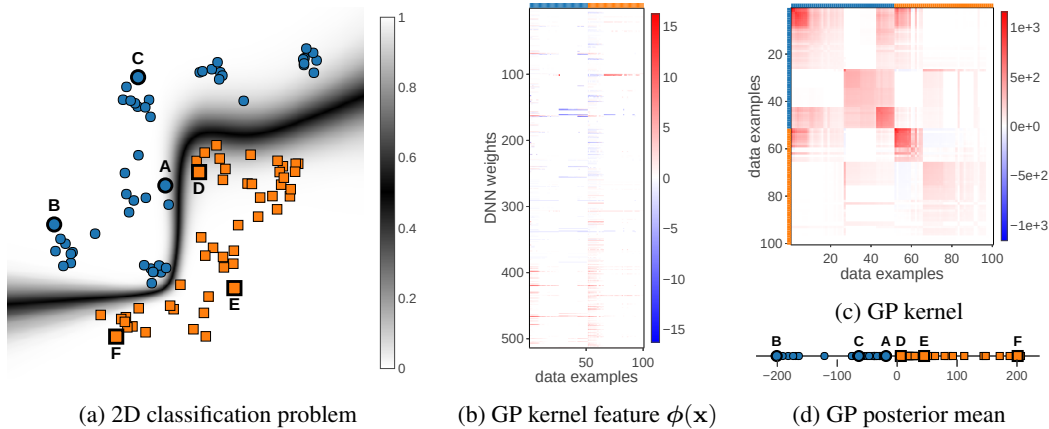


Figure 2: Fig. (a) shows a 2D binary-classification problem along with the predictive distribution of a DNN using 513 parameters. The corresponding feature and kernel matrices obtained using our approach are shown in (b) and (c), respectively (the two classes are grouped, and marked with blue and orange color along the axes). Fig. (d) shows the GP posterior mean where we see a clear separation between the two classes. Surprisingly, the border points A and D in (a) are also at the boundary in (d).

we can obtain GP kernels and nonlinear feature maps while training a DNN (see Fig. 2). Surprisingly, a GP kernel we derive is equivalent to the recently proposed neural tangent kernel (NTK) [8]. We present empirical results where we visualize the feature-map obtained on benchmark datasets such as MNIST and CIFAR, and demonstrate their use for DNN hyperparameter tuning. The code to reproduce our results is available at <https://github.com/team-approx-bayes/dnn2gp>. The work presented in this paper aims to facilitate further research on combining the strengths of DNNs and GPs in practical settings.

1.1 Related Work

The equivalence between infinitely-wide neural networks and GPs was originally discussed by Neal [16]. Subsequently, many works derived explicit expressions for the GP kernel corresponding to neural networks [4, 7, 16] and their deep variants [5, 6, 13, 18]. These works use a prior distribution on weights and derive kernels by averaging over the prior. Our work differs from these works in the fact that we use the *posterior* approximations to relate DNNs to GPs. Unlike these previous results, our results hold for DNNs of finite width.

A GP kernel we derive is equivalent to the recently proposed Neural Tangent Kernel (NTK) [8], which is obtained by using the Jacobian of the DNN outputs. For randomly initialized trajectories, as the DNN width goes to infinity, the NTK converges in probability to a deterministic kernel and remains asymptotically constant when training with gradient descent. Jacot et al. [8] motivate the NTK by using kernel gradient descent. Surprisingly, the NTK appears in our work with an entirely different approach where we consider approximations of the posterior distribution over weights. Due

to connections to the NTK, we expect similar properties for our kernel. Our approach additionally shows that we can obtain other types of kernels by using different approximate inference methods.

In a recent work, Lee et al. [14] derive the mean and covariance function corresponding to the GP induced by the NTK. Unfortunately, the model does not correspond to inference in a GP model (see Section 2.3.1 in their paper). Our approach does not have this issue and we can express Gaussian posterior approximations on a Bayesian DNN as inference in a GP regression model.

2 Deep Neural Networks (DNNs) and Gaussian Processes (GPs)

The goal of this paper is to present a theoretical relationship between training methods of DNNs and GPs. DNNs are typically trained by minimizing an empirical loss between the data and the predictions. For example, in supervised learning with a dataset $\mathcal{D} := \{(\mathbf{x}_i, \mathbf{y}_i)\}_{i=1}^N$ of N examples of input $\mathbf{x}_i \in \mathbb{R}^D$ and output $\mathbf{y}_i \in \mathbb{R}^K$, we can minimize a loss of the following form:

$$\bar{\ell}(\mathcal{D}, \mathbf{w}) := \sum_{i=1}^N \ell_i(\mathbf{w}) + \frac{1}{2} \delta \mathbf{w}^\top \mathbf{w}, \quad \text{where } \ell_i(\mathbf{w}) := \ell(\mathbf{y}_i, \mathbf{f}_w(\mathbf{x}_i)), \quad (1)$$

where $\mathbf{f}_w(\mathbf{x}) \in \mathbb{R}^K$ denotes the DNN outputs with weights $\mathbf{w} \in \mathbb{R}^P$, $\ell(\mathbf{y}, \mathbf{f}(\mathbf{x}))$ denotes a loss function between an output \mathbf{y} and the function $\mathbf{f}(\mathbf{x})$, and δ is a small L_2 regularizer.² We assume the loss function to be twice differentiable and strictly convex in \mathbf{f} (e.g., squared loss and cross-entropy loss). An attractive feature of DNNs is that they can be trained using stochastic-gradient (SG) methods [11]. Such methods scale well to large data settings.

GP models use an entirely different modeling approach which is based on directly modeling the functions rather than the parameters. For example, for regression problems with scalar outputs $y_i \in \mathbb{R}$, consider the following linear *basis-function* model with a nonlinear feature-map $\phi(\mathbf{x}) : \mathbb{R}^D \mapsto \mathbb{R}^P$:

$$y = \phi(\mathbf{x})^\top \mathbf{w} + \epsilon, \quad \text{with } \epsilon \sim \mathcal{N}(0, \sigma^2), \quad \text{and } \mathbf{w} \sim \mathcal{N}(0, \delta^{-1} \mathbf{I}_P), \quad (2)$$

where \mathbf{I}_P is a $P \times P$ identity matrix and σ^2 is the output noise variance. Defining the function to be $f(\mathbf{x}) := \phi(\mathbf{x})^\top \mathbf{w}$, the predictive distribution $p(f(\mathbf{x}_*) | \mathbf{x}_*, \mathcal{D})$ at a new test input \mathbf{x}_* is equal to that of the following model directly defined with a GP prior over $f(\mathbf{x})$ [23]:

$$y = f(\mathbf{x}) + \epsilon, \quad \text{with } f(\mathbf{x}) \sim \mathcal{GP}(0, \kappa(\mathbf{x}, \mathbf{x}')), \quad (3)$$

where $\kappa(\mathbf{x}, \mathbf{x}') := \mathbb{E}[f(\mathbf{x})f(\mathbf{x}')] = \delta^{-1} \phi(\mathbf{x})^\top \phi(\mathbf{x}')$ is the *covariance function* or *kernel* of the GP. The function-space model is more general in the sense that it can also deal with infinite-dimensional vector feature maps $\phi(\mathbf{x})$, giving us a *nonparametric* model. This view has been used to show that as a DNN becomes infinitely wide it tends to a GP, by essentially showing that averaging over $p(\mathbf{w})$ with the feature map induced by a DNN leads to a GP covariance function [16].

An attractive property of the *function-space* formulation as opposed to the *weight-space* formulation, such as (1), is that the posterior distribution has a closed-form expression. Another attractive property is that the posterior is usually unimodal, unlike the loss $\bar{\ell}(\mathcal{D}, \mathbf{w})$ which is typically nonconvex. Unfortunately, the computation of the posterior takes $O(N^3)$ which is infeasible for large datasets. GPs also require choosing a good kernel [23]. Unlike DNNs, inference in GPs remains much more difficult.

To summarize, despite the similarities between the two models, their training methods are fundamentally different. While DNNs employ stochastic optimization, GPs use closed-form updates. How can we relate these seemingly different training procedures in practical settings, e.g., without assuming infinite-width DNNs? In this paper, we provide an answer to this question. We derive theoretical results that relate the solutions and iterations of deep-learning algorithms to GP inference. We do so by first finding a Gaussian posterior approximation (Step A in Fig. 1), then use it to find a linear basis-function model (Step B in Fig. 1) and its corresponding GP (Step C in Fig. 1). We start in the next section with our first theoretical result.

²We can also assume that δ is small enough that it does not affect generalization of DNN.

3 Relating Minima of the Loss to GP Inference via Laplace Approximation

In this section, we present theoretical results relating minima of a deep-learning loss (1) to inference in GP models. A local minimizer \mathbf{w}_* of the loss (1) satisfies the following first-order and second-order conditions [17]: $\nabla_w \ell(\mathcal{D}, \mathbf{w}_*) = 0$ and $\nabla_{ww}^2 \ell(\mathcal{D}, \mathbf{w}_*) \succ 0$. Deep-learning optimizers, such as RMSprop and Adam, aim to find such minimizers, and our goal is to relate them to GP inference.

Step A (Laplace Approximation): To do so, we will use an approximate inference method called the Laplace approximation [1]. The minima of the loss (1) corresponds to a mode of the Bayesian model: $p(\mathcal{D}, \mathbf{w}) := \prod_{i=1}^N e^{-\ell_i(\mathbf{w})} p(\mathbf{w})$ with prior distribution $p(\mathbf{w}) := \mathcal{N}(\mathbf{w}|0, \delta^{-1} \mathbf{I}_P)$, assuming that the posterior is well-defined. The posterior distribution $p(\mathbf{w}|\mathcal{D}) = p(\mathcal{D}, \mathbf{w})/p(\mathcal{D})$ is usually computationally intractable and requires computationally-feasible approximation methods. The Laplace approximation uses the following Gaussian approximation for the posterior:

$$p(\mathbf{w}|\mathcal{D}) \approx \mathcal{N}(\mathbf{w}|\boldsymbol{\mu}, \boldsymbol{\Sigma}), \text{ where } \boldsymbol{\mu} = \mathbf{w}_* \text{ and } \boldsymbol{\Sigma}^{-1} = \sum_{i=1}^N \nabla_{ww}^2 \ell_i(\mathbf{w}_*) + \delta \mathbf{I}_P. \quad (4)$$

This approximation can be directly built using the solutions found by deep-learning optimizers.

Step B (Linear Model): The next step is to find a linear basis-function model whose posterior distribution is equal to the Gaussian approximation (4). We will now show that this is always possible whenever the gradient and Hessian of the loss³ can be approximated as follows:

$$\nabla_w \ell(\mathbf{w}) \approx \phi_w(\mathbf{x}) \mathbf{v}_w(\mathbf{x}, \mathbf{y}), \quad \nabla_{ww}^2 \ell(\mathbf{w}) \approx \phi_w(\mathbf{x}) \mathbf{D}_w(\mathbf{x}, \mathbf{y}) \phi_w(\mathbf{x})^\top, \quad (5)$$

where $\phi_w(\mathbf{x})$ is a $P \times Q$ feature matrix with Q as a positive integer, $\mathbf{v}_w(\mathbf{x}, \mathbf{y})$ is a Q length vector, and $\mathbf{D}_w(\mathbf{x}, \mathbf{y})$ is a $Q \times Q$ symmetric positive-definite matrix. We will now present results for a specific choice ϕ_w , \mathbf{v}_w , and \mathbf{D}_w . Our proof trivially generalizes to arbitrary choices of these quantities.

For the loss of form (1), the gradient and Hessian take the following form [15, 17]:

$$\nabla_w \ell(\mathbf{w}) = \mathbf{J}_w(\mathbf{x})^\top \mathbf{r}_w(\mathbf{x}, \mathbf{y}), \quad \nabla_{ww}^2 \ell(\mathbf{w}) = \mathbf{J}_w(\mathbf{x})^\top \boldsymbol{\Lambda}_w(\mathbf{x}, \mathbf{y}) \mathbf{J}_w(\mathbf{x}) + \mathbf{H}_f \mathbf{r}_w(\mathbf{x}, \mathbf{y}), \quad (6)$$

where $\mathbf{J}_w(\mathbf{x}) := \nabla_w \mathbf{f}_w(\mathbf{x})^\top$ is a $K \times P$ Jacobian matrix, $\mathbf{r}_w(\mathbf{x}, \mathbf{y}) := \nabla_f \ell(\mathbf{y}, \mathbf{f})$ is the *residual* vector evaluated at $\mathbf{f} := \mathbf{f}_w(\mathbf{x})$, $\boldsymbol{\Lambda}_w(\mathbf{x}, \mathbf{y}) := \nabla_{ff}^2 \ell(\mathbf{y}, \mathbf{f})$, referred to as the *noise precision*, is the $K \times K$ Hessian matrix of the loss evaluated at $\mathbf{f} := \mathbf{f}_w(\mathbf{x})$, and $\mathbf{H}_f := \nabla_{ww}^2 \mathbf{f}_w(\mathbf{x})$. The similarity between (5) and (6) is striking. In fact, if we ignore the second term for the Hessian $\nabla_{ww}^2 \ell(\mathbf{w})$ in (6), we get the well-known *Generalized Gauss-Newton* (GGN) approximation [15, 17]:

$$\nabla_{ww}^2 \ell(\mathbf{w}) \approx \mathbf{J}_w(\mathbf{x})^\top \boldsymbol{\Lambda}_w(\mathbf{x}, \mathbf{y}) \mathbf{J}_w(\mathbf{x}). \quad (7)$$

This gives us one choice for the approximation (5) where we can set $\phi_w(\mathbf{x}) := \mathbf{J}_w(\mathbf{x})^\top$, $\mathbf{v}_w(\mathbf{x}, \mathbf{y}) := \mathbf{r}_w(\mathbf{x}, \mathbf{y})$, and $\mathbf{D}_w(\mathbf{x}, \mathbf{y}) := \boldsymbol{\Lambda}_w(\mathbf{x}, \mathbf{y})$.

We are now ready to present our first theoretical result. Consider a Laplace approximation (4) but with the GGN approximation (7) for the Hessian. We refer to this as *Laplace-GGN*, and denote it by $\mathcal{N}(\mathbf{w}|\boldsymbol{\mu}, \tilde{\boldsymbol{\Sigma}})$ where $\tilde{\boldsymbol{\Sigma}}$ is the covariance obtained by using the GGN approximation. We denote the Jacobian, noise-precision, and residual at $\mathbf{w} = \mathbf{w}_*$ by $\mathbf{J}_*(\mathbf{x})$, $\boldsymbol{\Lambda}_*(\mathbf{x}, \mathbf{y})$, and $\mathbf{r}_*(\mathbf{x}, \mathbf{y})$. We construct a transformed dataset $\tilde{\mathcal{D}} = \{(\mathbf{x}_i, \tilde{\mathbf{y}}_i)\}_{i=1}^N$ where the outputs $\tilde{\mathbf{y}}_i \in \mathbb{R}^K$ are equal to $\tilde{\mathbf{y}}_i := \mathbf{J}_*(\mathbf{x}_i) \mathbf{w}_* - \boldsymbol{\Lambda}_*(\mathbf{x}_i, \mathbf{y}_i)^{-1} \mathbf{r}_*(\mathbf{x}_i, \mathbf{y}_i)$. We consider the following linear model for $\tilde{\mathcal{D}}$:

$$\tilde{\mathbf{y}} = \mathbf{J}_*(\mathbf{x}) \mathbf{w} + \boldsymbol{\epsilon}, \quad \text{with } \boldsymbol{\epsilon} \sim \mathcal{N}(0, (\boldsymbol{\Lambda}_*(\mathbf{x}, \mathbf{y}))^{-1}) \text{ and } \mathbf{w} \sim \mathcal{N}(0, \delta^{-1} \mathbf{I}_P). \quad (8)$$

The following theorem states our result.

Theorem 1. *The Laplace approximation $\mathcal{N}(\mathbf{w}|\boldsymbol{\mu}, \tilde{\boldsymbol{\Sigma}})$ is equal to the posterior distribution $p(\mathbf{w}|\tilde{\mathcal{D}})$ of the linear model (8).*

A proof is given in Appendix A.1. The linear model uses $\mathbf{J}_*(\mathbf{x})$ as the nonlinear feature map, and the noise prevision $\boldsymbol{\Lambda}_*(\mathbf{x}, \mathbf{y})$ is obtained using the Hessian of the loss evaluated at $\mathbf{f}_{w_*}(\mathbf{x})$. The model is constructed such that its posterior is equal to the Laplace approximation and it exploits the quadratic approximation at \mathbf{w}_* . We now describe the final step relating the linear model to GPs.

³For notational convenience, we sometime use $\ell(\mathbf{w})$ to denote $\ell(\mathbf{y}, \mathbf{f}_w(\mathbf{x}))$.

Step C (GP Model): To get a GP model, we use the equivalence between the weight-space view shown in (2) and the function-space view shown in (3). With this, we get the following GP regression model whose predictive distribution $p(f(\mathbf{x}_*)|\mathbf{x}_*, \tilde{\mathcal{D}})$ is equal to that of the linear model (8):

$$\tilde{\mathbf{y}} = \mathbf{f}(\mathbf{x}) + \epsilon, \quad \text{with } \mathbf{f}(\mathbf{x}) \sim \mathcal{GP}(0, \delta^{-1} \mathbf{J}_*(\mathbf{x}) \mathbf{J}_*(\mathbf{x}')^\top). \quad (9)$$

Note that the kernel here is a *multi-dimensional* $K \times K$ kernel. The steps A, B, and C together convert a DNN defined in the weight-space to a GP defined in the function-space. We refer to this approach as ‘‘DNN2GP’’.

The resulting GP predicts in the space of outputs $\tilde{\mathbf{y}}$ and therefore results in different predictions than the DNN, but it is connected to it through the Laplace approximation as shown in Theorem 1. In Appendix B, we describe prediction of the outputs \mathbf{y} (instead of $\tilde{\mathbf{y}}$) using this GP. Note that our approach leads to a heteroscedastic GP which could be beneficial. Even though our derivation assumes a Gaussian prior and DNN model, the approach holds for other types of priors and models.

Relationship to NTK: The GP kernel in (9) is the Neural Tangent Kernel⁴ (NTK) [8] which has desirable theoretical properties. As the width of the DNN is increasing to infinity, the kernel converges in probability to a deterministic kernel and also remains asymptotically constant during training. Our kernel is the NTK defined at \mathbf{w}_* and is expected to have similar properties. It is also likely that, as the DNN width is increased, the Laplace-GGN approximation has similar properties as a GP posterior, and can be potentially used to improve the performance of DNNs. For example, we can use GPs to tune hyperparameters of DNNs. The function-space view is also useful to understand relationships between data examples. Another advantage of our approach is that we can derive kernels other than the NTK. Any approximation of the form (5) will always result in a linear model similar to (8).

Accuracy of the GGN approximation: This approximation is accurate when the model $\mathbf{f}_w(\mathbf{x})$ can fit the data well, in which case the residuals $\mathbf{r}_w(\mathbf{x}, \mathbf{y})$ are close to zero for all training examples and the second term in (6) goes to zero [2, 15, 17]. The GGN approximation is a convenient option to derive DNN2GP, but, as it is clear from (5), other types of approximations can also be used.

4 Relating Iterations of a Deep-Learning Algorithm to GP Inference via VI

In this section, we present theoretical results relating iterations of an RMSprop-like algorithm to GP inference. The RMSprop algorithm [21] uses the following updates (all operations are element-wise):

$$\mathbf{w}_{t+1} \leftarrow \mathbf{w}_t - \alpha_t (\sqrt{\mathbf{s}_{t+1}} + \Delta)^{-1} \hat{\mathbf{g}}(\mathbf{w}_t), \quad \mathbf{s}_{t+1} \leftarrow (1 - \beta_t) \mathbf{s}_t + \beta_t (\hat{\mathbf{g}}(\mathbf{w}_t))^2, \quad (10)$$

where t is the iteration, $\alpha_t > 0$ and $0 < \beta_t < 1$ are learning rates, $\Delta > 0$ is a small scalar, and $\hat{\mathbf{g}}(\mathbf{w})$ is a stochastic-gradient estimate for $\ell(\mathcal{D}, \mathbf{w})$ obtained using minibatches. Our goal is to relate the iterates \mathbf{w}_t to GP inference using our DNN2GP approach, but this requires a posterior approximation defined at each \mathbf{w}_t . We cannot use the Laplace approximation because it is only valid at \mathbf{w}_* . We will instead use a version of RMSprop proposed in [10] for variational inference (VI), which will enable us to construct a GP inference at each \mathbf{w}_t .

Step A (Variational Inference): The variational online-Newton (VON) algorithm proposed in [10] optimizes the variational objective, but takes an algorithmic form similar to RMSprop (see a detailed discussion in [10]). Below, we show a batch version of VON, derived using Eq. (54) in [10]:

$$\boldsymbol{\mu}_{t+1} \leftarrow \boldsymbol{\mu}_t - \beta_t (\mathbf{S}_{t+1} + \delta \mathbf{I}_P)^{-1} \mathbb{E}_{q_t(\mathbf{w})} [\nabla_w \bar{\ell}(\mathcal{D}, \mathbf{w})], \quad (11)$$

$$\mathbf{S}_{t+1} \leftarrow (1 - \beta_t) \mathbf{S}_t + \beta_t \sum_{i=1}^N \mathbb{E}_{q_t(\mathbf{w})} [\nabla_{ww}^2 \ell_i(\mathbf{w})], \quad (12)$$

where \mathbf{S}_t is a scaling matrix similar to the scaling vector \mathbf{s}_t in RMSprop, and the Gaussian approximation at iteration t is defined as $q_t(\mathbf{w}) := \mathcal{N}(\mathbf{w} | \boldsymbol{\mu}_t, \boldsymbol{\Sigma}_t)$ where $\boldsymbol{\Sigma}_t := (\mathbf{S}_t + \delta \mathbf{I}_P)^{-1}$. Since there are no closed-form expressions for the expectations, the Monte Carlo (MC) approximation is used.

Step B (Linear Model): As before, we assume the choices for (5) obtained by using the GGN approximation (7). We consider the variant for VON where the GGN approximation is used for the Hessian and MC approximation is used for the expectations with respect to $q_t(\mathbf{w})$. We call this the

⁴The NTK corresponds to $\delta = 1$ which implies a standard normal prior on weights.

Variational Online GGN or VOGGN algorithm. A similar algorithms have recently been used in [19] where it shows competitive performance to Adam and SGD.

We now present a theorem relating iterations of VOGGN to linear models. We denote the Gaussian approximation obtained at iteration t by $\tilde{q}_t(\mathbf{w}) := \mathcal{N}(\mathbf{w}|\boldsymbol{\mu}_t, \tilde{\boldsymbol{\Sigma}}_t)$ where $\tilde{\boldsymbol{\Sigma}}_t$ is used to emphasize the GGN approximation used in VOGGN. We present theoretical results for VOGGN with 1 MC sample which is denoted by $\mathbf{w}_t \sim \tilde{q}_t(\mathbf{w})$. Our proof in Appendix A.2 discusses a more general setting with multiple MC samples. Similarly to the previous section, we first define a transformed dataset: $\tilde{\mathcal{D}}_t := \{(\mathbf{x}_i, \tilde{\mathbf{y}}_{i,t})\}_{i=1}^N$ where $\tilde{\mathbf{y}}_{i,t} := \mathbf{J}_{w_t}(\mathbf{x}_i)\mathbf{w}_t - \boldsymbol{\Lambda}_{w_t}(\mathbf{x}_i, \mathbf{y}_i)^{-1}\mathbf{r}_{w_t}(\mathbf{x}_i, \mathbf{y}_i)$, and then a linear basis-function model:

$$\tilde{\mathbf{y}}_t = \mathbf{J}_{w_t}(\mathbf{x})\mathbf{w} + \epsilon, \quad \text{with } \epsilon \sim \mathcal{N}(0, (\beta_t \boldsymbol{\Lambda}_{w_t}(\mathbf{x}, \mathbf{y}))^{-1}) \text{ and } \mathbf{w} \sim \mathcal{N}(\mathbf{m}_t, \mathbf{V}_t) \quad (13)$$

with $\mathbf{V}_t^{-1} := (1 - \beta_t)\tilde{\boldsymbol{\Sigma}}_t^{-1} + \beta_t\delta\mathbf{I}_P$ and $\mathbf{m}_t := (1 - \beta_t)\mathbf{V}_t\tilde{\boldsymbol{\Sigma}}_t^{-1}\mathbf{w}_t$. The model is very similar to the one obtained for Laplace approximation, but is now defined using the iterates \mathbf{w}_t instead of the minimum \mathbf{w}_* . The prior over \mathbf{w} is not the standard Gaussian anymore, rather a correlated Gaussian derived from $q_t(\mathbf{w})$. The theorem below states the result (a proof is given in Appendix A.2).

Theorem 2. *The Gaussian approximation $\mathcal{N}(\mathbf{w}|\mathbf{w}_{t+1}, \tilde{\boldsymbol{\Sigma}}_{t+1})$ at iteration $t + 1$ of the VOGGN update is equal to the posterior distribution $p(\mathbf{w}|\tilde{\mathcal{D}}_t)$ of the linear model (13).*

Step C (GP Model): The linear model (13) has the same predictive distribution as the GP below:

$$\tilde{\mathbf{y}}_t = \mathbf{f}_t(\mathbf{x}) + \epsilon, \quad \text{with } \mathbf{f}_t(\mathbf{x}) \sim \mathcal{GP}(\mathbf{J}_{w_t}(\mathbf{x})\mathbf{m}_t, \mathbf{J}_{w_t}(\mathbf{x})\mathbf{V}_t\mathbf{J}_{w_t}(\mathbf{x}')^\top). \quad (14)$$

The kernel here is similar to the NTK but now there is a covariance term \mathbf{V}_t which incorporates the effect of the previous $q_t(\mathbf{w})$ as a prior. Our DNN2GP approach shows that one iteration of VOGGN in the weight-space is equivalent to inference in a GP regression model defined in a transformed function-space with respect to a kernel similar to the NTK. This can be compared with the results in [8], where learning by plain gradient descent is shown to be equivalent to kernel gradient descent in the function-space. Similarly to the Laplace case, the resulting GP predicts in the space of outputs $\tilde{\mathbf{y}}_t$, but predictions for \mathbf{y}_t can be obtained using a method described in Appendix B.

A Deep-Learning Optimizer Derived from VOGGN: The VON algorithm, even though similar to RMSprop, does not converge to the minimum of the loss. This is because it optimizes the variational objective. Fortunately, a slight modification of this algorithm gives us a deep-learning optimizer which is similar to RMSprop but is guaranteed to converge to the minimum of the loss. For this, we approximate the expectations in the updates (11)-(12) at the mean $\boldsymbol{\mu}_t$. This is called the *zeroth-order delta approximation*; see Appendix A.6 in [9] for details of this method. Using this approximation and denoting the mean $\boldsymbol{\mu}_t$ by \mathbf{w}_t , we get the following update:

$$\mathbf{w}_{t+1} \leftarrow \mathbf{w}_t - \beta_t(\hat{\mathbf{S}}_{t+1} + \delta\mathbf{I}_P)^{-1}\nabla_{\mathbf{w}}\bar{\ell}(\mathcal{D}, \mathbf{w}_t), \quad \hat{\mathbf{S}}_{t+1} \leftarrow (1 - \beta_t)\hat{\mathbf{S}}_t + \beta_t \sum_{i=1}^N [\nabla_{\mathbf{w}\mathbf{w}}^2 \ell_i(\mathbf{w}_t)].$$

We refer to this as Online GGN or OGGN method. A fixed point \mathbf{w}_* of this iteration is also a minimizer of the loss since we have $\nabla_{\mathbf{w}}\bar{\ell}(\mathcal{D}, \mathbf{w}_*) = 0$. Unlike RMSprop, at each iteration, we still get a Gaussian approximation $\hat{q}_t(\mathbf{w}) := \mathcal{N}(\mathbf{w}|\mathbf{w}_t, \hat{\boldsymbol{\Sigma}}_t)$ with $\hat{\boldsymbol{\Sigma}}_t := (\hat{\mathbf{S}}_t + \delta\mathbf{I}_P)^{-1}$. Therefore, the posterior of the linear model from Theorem (2) is equivalent to \hat{q}_t when $\tilde{\boldsymbol{\Sigma}}_t$ is replaced by $\hat{\boldsymbol{\Sigma}}_t$ (see Appendix A.3). In conclusion, by using VI in our DNN2GP approach, we are able to relate the iterations of a deep-learning optimizer to GP inference.

Implementation of DNN2GP: In practice, both VOGGN and OGGN are more computationally expensive than RMSprop because they both involve computation of full covariance matrices. To address this issue, we simply use the diagonal versions of these algorithms discussed in [10, 19]. Specifically, we use the VOGN and OGN algorithms discussed in [19]. This implies that \mathbf{V}_t is a diagonal matrix and the GP kernel can be obtained without requiring any computation of large matrices. Only Jacobian computations are required. In our experiments, we also resort to computing the kernel over a subset of data instead of the whole data, which further reduces the cost.

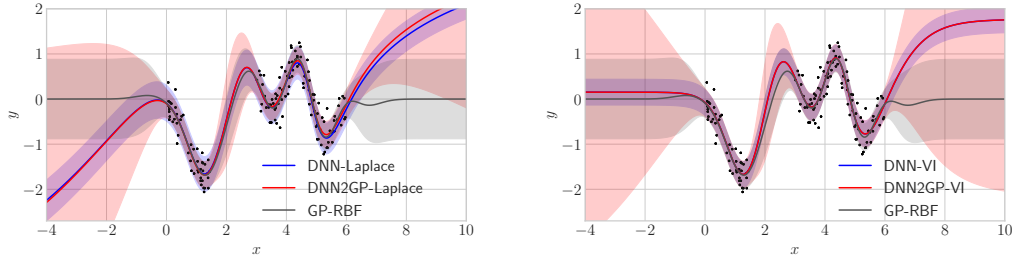


Figure 3: This figure shows a visualization of the predictive distributions on a modified version of the Snelson dataset [20]. The left figure shows Laplace and the right one shows VI. DNN2GP is our proposed method, elaborated upon in Appendix B, while DNN refers to a diagonal Gaussian approximation. We also compare to a GP with RBF kernel (GP-RBF). An MLP is used for DNN2GP and DNN. We see that, wherever the data is missing, the uncertainties are larger for our method than the others. For classification, we give an example in Fig. 9 in the appendix.

5 Experimental Results

5.1 Comparison of DNN2GP Uncertainty

In this section, we visualize the quality of the uncertainty of the GP obtained with our DNN2GP approach on a simple regression task. To approximate predictive uncertainty for our approach, we use the method described in Appendix B. We use both Laplace and VI approximations, referred to as ‘DNN2GP-Laplace’ and ‘DNN2GP-VI’, respectively. We compare it to the uncertainty obtained by using the MC approximation in DNN (referred to as ‘DNN-Laplace’ and ‘DNN-VI’). We also compare to a standard GP regression model with a RBF kernel (refer to as ‘GP-RBF’), whose kernel hyperparameters are chosen by optimizing the GP marginal likelihood.

We consider a version of the Snelson dataset [20] where, to assess the ‘in-between’ uncertainty, we remove the data points between $x = 1.5$ and $x = 3$. We use a single hidden-layer MLP with 32 units and sigmoidal transfer function. Fig. 3 shows the results for Laplace (left) and VI (right) approximation. For Laplace, we use Adam [11], and, for VI, we use VOGN [10]. The uncertainty provided by DNN2GP is bigger than the other methods wherever the data is not observed. In our approach, the spread is more for VI than for Laplace.

5.2 GP Kernel and Predictive Distribution for Classification Datasets

In this section, we visualize the GP kernel and predictive distribution for DNNs trained on CIFAR-10 and MNIST. Our goal is to show that our GP kernel and its predictions enhance our understanding of DNN’s performance on classification tasks. We consider LeNet-5 [12] and compute both the Laplace and VI approximations. We show the visualization at the posterior mean of the Gaussian approximation.

The $K \times K$ GP kernel $\kappa_*(\mathbf{x}, \mathbf{x}') := \mathbf{J}_*(\mathbf{x})\mathbf{J}_*(\mathbf{x}')^\top$ results in a kernel matrix of dimensionality $NK \times NK$ which makes it difficult to visualize for our datasets. To simplify, we compute the sum of the diagonal entries of $\kappa_*(\mathbf{x}, \mathbf{x}')$ to get an $N \times N$ matrix. This corresponds to modelling the output for each class with an individual GP and then summing the kernels of these GPs. We also visualize the GP posterior mean: $\mathbb{E}[\mathbf{f}(\mathbf{x})|\mathcal{D}] = \mathbb{E}[\mathbf{J}_*(\mathbf{x})\mathbf{w}|\mathcal{D}] = \mathbf{J}_*(\mathbf{x})\mathbf{w}_* \in \mathbb{R}^K$. and use the reparameterization that allows to predict in the data space \mathbf{y} instead of $\tilde{\mathbf{y}}$ which is explained in Appendix B.

Fig. 4a shows the GP kernel matrix and the posterior mean for the Laplace approximation on MNIST. The rows and columns containing 300 data examples are grouped according to the classes. The kernel matrix clearly shows the correlations learned by the DNN. As expected, each row in the posterior mean also reflects that the classes are correctly classified (DNN test accuracy is 99%). Fig. 4b shows the GP posterior mean after reparameterization for CIFAR-10 where we see a more noisy pattern due to a lower accuracy of around 68% on this task.

Fig. 4d shows the two components of the predictive variances that can be interpreted as ‘‘aleatoric’’ and ‘‘epistemic’’ uncertainty. As shown in Eq. (48) in Appendix B.2, for a multiclass classification loss, the variance of the prediction of a label at an input \mathbf{x}_* is equal to $\Lambda_*(\mathbf{x}_*) + \Lambda_*(\mathbf{x}_*)\mathbf{J}_*(\mathbf{x}_*)\tilde{\Sigma}\mathbf{J}_*(\mathbf{x}_*)^\top\Lambda_*(\mathbf{x}_*)$. Similar to the linear basis function model, the two terms here have

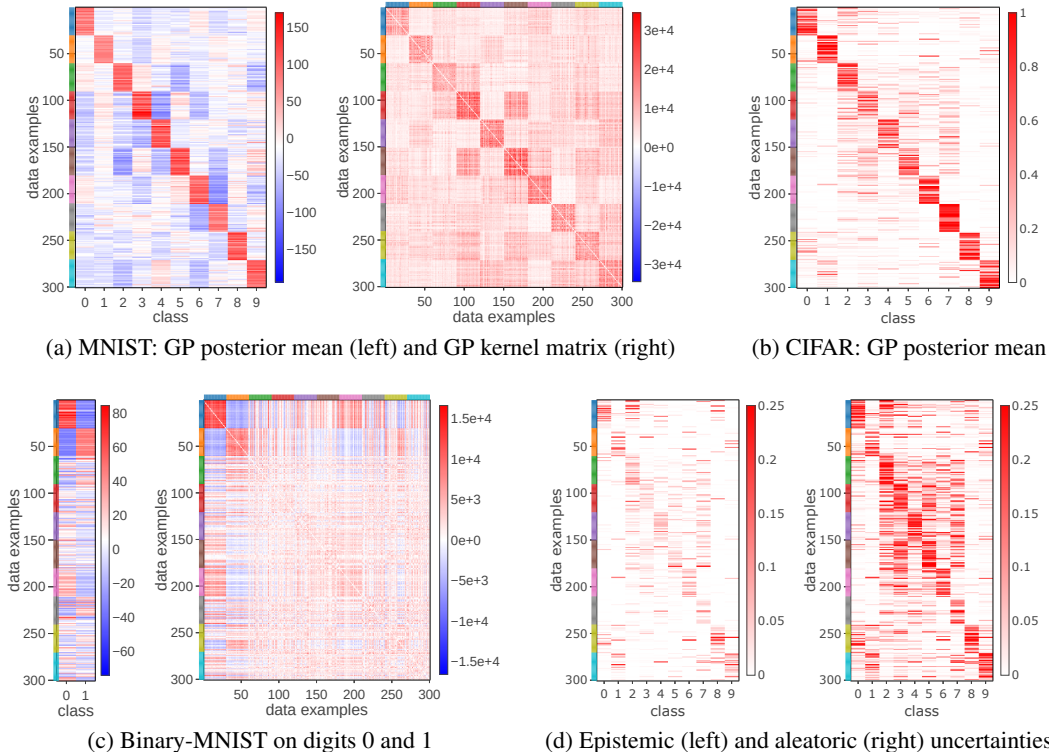


Figure 4: DNN2GP kernels, posterior means and uncertainties with LeNet5 of 300 samples on binary MNIST in Fig. (c), MNIST in Fig. (a), and CIFAR-10 in Fig. (b,d). The colored regions on the y-axis mark the classes. Fig. (a) shows the kernel and the predictive mean for the Laplace approximation, which gives 99% test accuracy. We see in the kernel that examples with same class labels are correlated. Fig. (c) shows the same for binary MNIST trained only on digits 0 and 1 by using VI. The kernel clearly shows the out-of-class predictive behavior where predictions are not certain. Fig. (b) and (d) show the Laplace-GP on the more complex CIFAR-10 data set where we obtain 68% accuracy. Fig. (d) shows the two components of the predictive variance for CIFAR-10 that can be interpreted as epistemic (left) and aleatoric (right) uncertainties. The estimated epistemic uncertainty is much lower than the aleatoric uncertainty, implying that the model is not flexible enough. This is plausible since the accuracy of the model is not too high (merely 68%).

an interpretation (e.g., see [1] Eq. 3.59). The first term can be interpreted as the aleatoric uncertainty (label noise), while the second term takes a form that resembles the epistemic uncertainty (model noise). Fig. 4d shows these for CIFAR-10 where we see that the uncertainty of the model is low (left) and the label noise rather high (right). This interpretation then implies that the model is unable to flexibly model the data, thereby giving a high label noise.

In Fig. 4c, we study the kernel for classes *outside* of the training dataset using VI. We train LeNet-5 on digits 0 and 1 with VOGN and visualize the predictive mean and kernel on all 10 classes denoted by differently colored regions on the y-axis. We can see that there are slight correlations to the out-of-class samples but no overconfident predictions. In contrast, the pattern between 0 and 1 and is quite strong. The kernel obtained with DNN2GP helps to interpret and visualize such correlations.

5.3 Tuning the Hyperparameters of a DNN Using the GP Marginal Likelihood

In this section, we demonstrate the tuning of DNN hyperparameters by using the GP marginal likelihood on a real and synthetic regression dataset. In the deep-learning literature, this is usually done by analyzing loss on the validation set. Our goal is to demonstrate that with DNN2GP we can do this by simply computing marginal likelihoods on the *training* set alone.

We generate a synthetic regression dataset ($N = 100$) with 1 dimensional inputs and a scalar output (see Fig. 5) where there are a few data points around $x = 0$ but plenty away from it. We fit the data by using a neural network with single hidden layer of 20 units and tanh-nonlinearity. Our goal is to

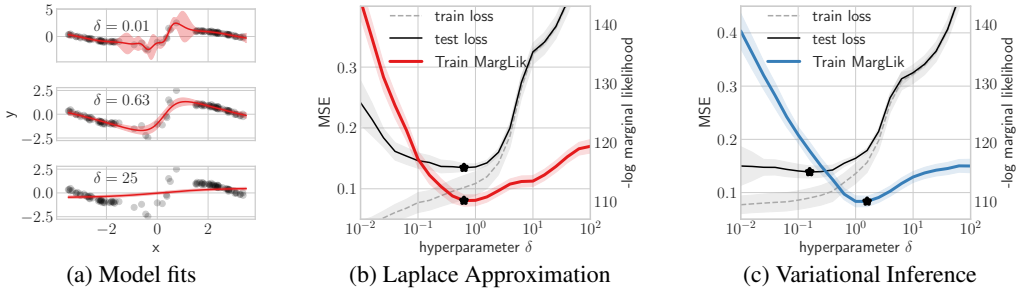


Figure 5: This figure demonstrates the use of the GP marginal likelihood to tune hyperparameters of a DNN. We tune the regularization parameter δ on a synthetic dataset shown in (a). Fig. (b) and (c) show train and test MSE along with log of the marginal likelihoods on training data obtained with Laplace and VI respectively. We show the standard error over 10 runs. We clearly see that best hyperparameters (shown with black star) found by test loss or small generalization gap and marginal-likelihood match well.

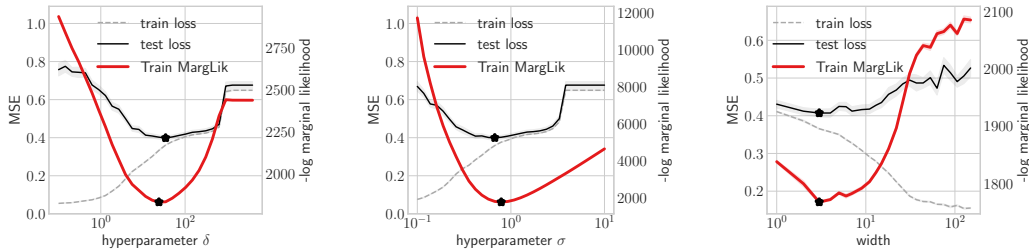


Figure 6: This is same as Fig. 5 but on a real dataset: UCI Red Wine Quality. All the plots use Laplace approximation, and the standard errors are estimated over 20 splits. We tune the following hyperparameters: the regularization parameter δ (left), the noise-variance σ (middle), and the DNN width (right). The train log marginal-likelihood chooses hyperparameters that give a low test error.

tune the regularization parameter δ to trade-off underfitting vs overfitting. Fig. 5b and 5c show the train log marginal-likelihood obtained with the GP obtained by DNN2GP, alongwith the test and train mean-square error (MSE) obtained using a point estimate. Black stars indicate the hyperparameters chosen by using the test loss and log marginal likelihood, respectively. We clearly see that the train marginal-likelihood chooses hyperparameters that give low test error. The train MSE on the other hand overfits as δ is reduced.

Next, we discuss results for a real dataset: UCI Red Wine Quality ($N = 1599$) with an input-dimensionality of 12 and a scalar output. We use an MLP with 2 hidden layers 20 units each and tanh transfer function. We consider tuning the following hyperparameters: the regularization parameter δ , the noise-variance σ , and the DNN width. The last parameters is a discrete parameter. We use Laplace approximation and tune one parameter at a time while keeping the others fixed (we use $\delta = 30$, $\sigma = 0.64$, and $\sigma = 0.64$, $\delta = 3$). Similarly to the synthetic data case, the train marginal-likelihood selects hyperparameters than give low test error. These experiments show that the DNN2GP framework can be useful to tune DNN hyperparameters, although this needs to be confirmed for larger networks than we used here.

6 Discussion and Future Work

In this paper, we present theoretical results connecting approximate inference on DNNs to GP posteriors. Our work enables the extraction of feature maps and GP kernels by simply training DNNs. It provides a natural way to combine the two different models.

Our hope is that our theoretical results will facilitate further research on combining strengths of DNNs and GPs. A computational bottleneck is the Jacobian computation which prohibits application to large problems. There are several ways to reduce this computation, e.g., by choosing a different type of GGN approximation that uses gradients instead of the Jacobians. Exploration of such methods is a future direction that needs to be pursued.

Exact inference on the GP model we derive is still computationally infeasible for large problems. However, further approximations could enable inference on bigger datasets. Finally, our work opens many other interesting avenues where a combination of GPs and DNNs can be useful. For example, hyperparameter tuning, Bandits, deep reinforcement learning, Bayesian optimization, active learning, interpretation, etc. We hope that our work enables the community to conduct further research on such problems.

Acknowledgements

We would like to thank Kazuki Osawa (Tokyo Institute of Technology), Anirudh Jain (RIKEN), and Runa Eschenhagen (RIKEN) for their help with the experiments. We would also like to thank Matthias Bauer (DeepMind) for discussions and useful feedback. Many thanks to Roman Bachmann (RIKEN) for helping with the visualization in Fig. 1. We also thank Stephan Mandt (UCI) for suggesting the marginal likelihood experiment. We thank the reviewers and the area chair for their feedback as well. We are also thankful for the RAIDEN computing system and its support team at the RIKEN Center for Advanced Intelligence Project which we used extensively for our experiments.

References

- [1] Christopher M Bishop. *Pattern recognition and machine learning*. springer, 2006.
- [2] L. Bottou, F. Curtis, and J. Nocedal. Optimization methods for large-scale machine learning. *SIAM Review*, 60(2):223–311, 2018. doi: 10.1137/16M1080173.
- [3] John Bradshaw, Alexander G de G Matthews, and Zoubin Ghahramani. Adversarial examples, uncertainty, and transfer testing robustness in Gaussian process hybrid deep networks. *arXiv preprint arXiv:1707.02476*, 2017.
- [4] Youngmin Cho and Lawrence K. Saul. Kernel methods for deep learning. In Y. Bengio, D. Schuurmans, J. D. Lafferty, C. K. I. Williams, and A. Culotta, editors, *Advances in Neural Information Processing Systems 22*, pages 342–350. Curran Associates, Inc., 2009.
- [5] Alexander G. de G. Matthews, Jiri Hron, Mark Rowland, Richard E. Turner, and Zoubin Ghahramani. Gaussian process behaviour in wide deep neural networks. In *International Conference on Learning Representations*, 2018.
- [6] Adrià Garriga-Alonso, Carl Edward Rasmussen, and Laurence Aitchison. Deep convolutional networks as shallow Gaussian processes. In *International Conference on Learning Representations*, 2019.
- [7] Tamir Hazan and Tommi S. Jaakkola. Steps toward deep kernel methods from infinite neural networks. *CoRR*, abs/1508.05133, 2015.
- [8] Arthur Jacot, Franck Gabriel, and Clement Hongler. Neural tangent kernel: Convergence and generalization in neural networks. In S. Bengio, H. Wallach, H. Larochelle, K. Grauman, N. Cesa-Bianchi, and R. Garnett, editors, *Advances in Neural Information Processing Systems 31*, pages 8571–8580. Curran Associates, Inc., 2018.
- [9] Mohammad Khan. *Variational learning for latent Gaussian model of discrete data*. PhD thesis, University of British Columbia, 2012.
- [10] Mohammad Emtiyaz Khan, Didrik Nielsen, Voot Tangkaratt, Wu Lin, Yarin Gal, and Akash Srivastava. Fast and scalable Bayesian deep learning by weight-perturbation in Adam. In *International Conference on Machine Learning*, pages 2616–2625, 2018.
- [11] Diederik P Kingma and Jimmy Ba. Adam: A method for stochastic optimization. *arXiv preprint arXiv:1412.6980*, 2014.
- [12] Yann LeCun, Léon Bottou, Yoshua Bengio, Patrick Haffner, et al. Gradient-based learning applied to document recognition. *Proceedings of the IEEE*, 86(11):2278–2324, 1998.

- [13] Jaehoon Lee, Yasaman Bahri, Roman Novak, Samuel S. Schoenholz, Jeffrey Pennington, and Jascha Sohl-Dickstein. Deep neural networks as Gaussian processes. In *6th International Conference on Learning Representations, ICLR 2018, Vancouver, BC, Canada, April 30 - May 3, 2018, Conference Track Proceedings*, 2018.
- [14] Jaehoon Lee, Lechao Xiao, Samuel S. Schoenholz, Yasaman Bahri, Roman Novak, Jascha Sohl-Dickstein, and Jeffrey Pennington. Wide Neural Networks of Any Depth Evolve as Linear Models Under Gradient Descent. *arXiv e-prints*, art. arXiv:1902.06720, Feb 2019.
- [15] James Martens. New perspectives on the natural gradient method. *CoRR*, abs/1412.1193, 2014.
- [16] Radford M. Neal. *Bayesian Learning for Neural Networks*. Springer-Verlag, Berlin, Heidelberg, 1996. ISBN 0387947248.
- [17] Jorge Nocedal and Stephen Wright. *Numerical optimization*. Springer Science & Business Media, 2006.
- [18] Roman Novak, Lechao Xiao, Yasaman Bahri, Jaehoon Lee, Greg Yang, Daniel A. Abolafia, Jeffrey Pennington, and Jascha Sohl-dickstein. Bayesian deep convolutional networks with many channels are Gaussian processes. In *International Conference on Learning Representations*, 2019.
- [19] Kazuki Osawa, Siddharth Swaroop, Anirudh Jain, Runa Eschenhagen, Richard Turner, Rio Yokota, and Mohammad Emtiyaz Khan. Practical deep learning with Bayesian principles. In *Advances in Neural Information Processing Systems*, 2019.
- [20] Edward Snelson and Zoubin Ghahramani. Sparse gaussian processes using pseudo-inputs. In Y. Weiss, B. Schölkopf, and J. C. Platt, editors, *Advances in Neural Information Processing Systems 18*, pages 1257–1264. MIT Press, 2006.
- [21] Tijmen Tieleman and Geoffrey Hinton. Lecture 6.5-RMSprop: Divide the gradient by a running average of its recent magnitude. *COURSERA: Neural Networks for Machine Learning 4*, 2012.
- [22] Christopher KI Williams. Computing with infinite networks. In *Advances in neural information processing systems*, pages 295–301, 1997.
- [23] Christopher KI Williams and Carl Edward Rasmussen. *Gaussian processes for machine learning*, volume 2. MIT Press Cambridge, MA, 2006.

A Proofs

In this section, we prove the theorems presented in the main text.

A.1 Proof of Theorem 1

We begin with the Gaussian approximation of the Laplace approximation. We will then express its natural parameters in terms of the gradient and Hessians. Application of the GGN approximation and some further manipulation will show that the distribution correspond to the posterior of a linear model.

We start with the Laplace approximation (4) and express its natural parameters in terms of the gradient and Hessians. We denote the natural-parameters of this Gaussian approximation $\mathcal{N}(\mathbf{w}|\boldsymbol{\mu}, \boldsymbol{\Sigma})$ by $\boldsymbol{\eta} := \{\boldsymbol{\Sigma}^{-1}\boldsymbol{\mu}, -\frac{1}{2}\boldsymbol{\Sigma}^{-1}\}$. In (4), the second natural parameter is set to the following which is written in terms of the Hessian:

$$-\frac{1}{2}\boldsymbol{\Sigma}^{-1} = -\frac{1}{2} \left[\sum_{i=1}^N \nabla_{\mathbf{w}\mathbf{w}}^2 \ell_i(\mathbf{w}_*) + \delta \mathbf{I}_P \right]. \quad (15)$$

We can also express the first natural parameter in terms of the gradient and Hessians as shown below. We use the first-order stationary condition, that is, $\nabla_{\mathbf{w}} \bar{\ell}(\mathcal{D}, \mathbf{w}_*) = 0$. Adding $\boldsymbol{\Sigma}^{-1}\boldsymbol{\mu}$ to the both sides of this condition, we get the following:

$$\boldsymbol{\Sigma}^{-1}\boldsymbol{\mu} = -\nabla_{\mathbf{w}} \bar{\ell}(\mathcal{D}, \mathbf{w}_*) + \boldsymbol{\Sigma}^{-1}\boldsymbol{\mu} \quad (16)$$

$$= -\sum_{i=1}^N \nabla_{\mathbf{w}} \ell_i(\mathbf{w}_*) - \delta \mathbf{w}_* + \left[\sum_{i=1}^N \nabla_{\mathbf{w}\mathbf{w}}^2 \ell_i(\mathbf{w}_*) + \delta \mathbf{I}_P \right] \mathbf{w}_* \quad (17)$$

$$= \sum_{i=1}^N \left[-\nabla_{\mathbf{w}} \ell_i(\mathbf{w}_*) + \nabla_{\mathbf{w}\mathbf{w}}^2 \ell_i(\mathbf{w}_*) \mathbf{w}_* \right], \quad (18)$$

where in the second step, we substitute $\boldsymbol{\mu}$ by \mathbf{w}_* and also use (15). With this, both natural parameters are now expressed in terms of the gradient and Hessian.

We will now substitute these in the Laplace approximation, denoted by $q_L(\mathbf{w}) := \mathcal{N}(\mathbf{w}|\boldsymbol{\mu}, \boldsymbol{\Sigma})$. Using (15) and (18), we get the following expression:

$$q_L(\mathbf{w}) = \frac{1}{\sqrt{(2\pi)^P |\boldsymbol{\Sigma}|}} \exp \left[-\frac{1}{2} (\mathbf{w} - \boldsymbol{\mu})^\top \boldsymbol{\Sigma}^{-1} (\mathbf{w} - \boldsymbol{\mu}) \right] \quad (19)$$

$$\propto \exp \left[-\frac{1}{2} \mathbf{w}^\top (\boldsymbol{\Sigma}^{-1}) \mathbf{w} + \mathbf{w}^\top (\boldsymbol{\Sigma}^{-1} \boldsymbol{\mu}) \right] \quad (20)$$

$$= \exp \left(\frac{-\delta \mathbf{w}^\top \mathbf{w}}{2} \right) \prod_{i=1}^N \exp \left[-\frac{1}{2} \mathbf{w}^\top \nabla_{\mathbf{w}\mathbf{w}}^2 \ell_i(\mathbf{w}_*) \mathbf{w} + \mathbf{w}^\top \left\{ -\nabla_{\mathbf{w}} \ell_i(\mathbf{w}_*) + \nabla_{\mathbf{w}\mathbf{w}}^2 \ell_i(\mathbf{w}_*) \mathbf{w}_* \right\} \right], \quad (21)$$

where in the last line we use (15) and (18).

Now, we will employ the GGN approximation (7) which gives us the Laplace-GGN approximation $\mathcal{N}(\mathbf{w}|\boldsymbol{\mu}, \tilde{\boldsymbol{\Sigma}})$, shown below:

$$\exp \left(\frac{-\delta \mathbf{w}^\top \mathbf{w}}{2} \right) \prod_{i=1}^N \exp \left[\frac{-1}{2} \mathbf{w}^\top \mathbf{J}_*(\mathbf{x}_i)^\top \boldsymbol{\Lambda}_{i,*} \mathbf{J}_*(\mathbf{x}_i) \mathbf{w} + \mathbf{w}^\top \mathbf{J}_*(\mathbf{x}_i)^\top \left\{ \boldsymbol{\Lambda}_{i,*} \mathbf{J}_*(\mathbf{x}_i) \mathbf{w}_* - \mathbf{r}_{i,*} \right\} \right], \quad (22)$$

where for notational convenience we have denoted $\boldsymbol{\Lambda}_{i,*} := \boldsymbol{\Lambda}_*(\mathbf{x}_i, \mathbf{y}_i)$ and $\mathbf{r}_{i,*} := \mathbf{r}_*(\mathbf{x}_i, \mathbf{y}_i)$.

A key point here is that each term in the product over i in (22) is proportional to a Gaussian distribution, provided that $\boldsymbol{\Lambda}_{i,*} \succ 0$, which is the case since we assume the loss function to be strictly convex. We will now express each term in the product, as a likelihood over a *pseudo-output* defined as $\tilde{\mathbf{y}}_i := \mathbf{J}_*(\mathbf{x}_i) \mathbf{w}_* - \boldsymbol{\Lambda}_{i,*}^{-1} \mathbf{r}_{i,*}$. Using this and completing the square within each term in the product over i in (22), we get the following:

$$\tilde{q}_L(\mathbf{w}) := \mathcal{N}(\mathbf{w}|\boldsymbol{\mu}, \tilde{\boldsymbol{\Sigma}}) \propto \mathcal{N}(\mathbf{w}|0, \delta^{-1} \mathbf{I}_P) \prod_{i=1}^N \mathcal{N}(\tilde{\mathbf{y}}_i | \mathbf{J}_*(\mathbf{x}_i) \mathbf{w}, \boldsymbol{\Lambda}_{i,*}^{-1}). \quad (23)$$

The right hand side of the above equation is proportional to the posterior distribution $p(\mathbf{w}|\tilde{\mathcal{D}})$ given a transformed dataset $\tilde{\mathcal{D}} := \{(\mathbf{x}_i, \tilde{\mathbf{y}}_i)\}_{i=1}^N$ of a linear basis-function model $\tilde{\mathbf{y}} = \mathbf{J}_*(\mathbf{x})\mathbf{w} + \epsilon$ with Gaussian noise $\epsilon \sim \mathcal{N}(0, (\mathbf{\Lambda}_*(\mathbf{x}, \mathbf{y}))^{-1})$ and prior distribution $\mathbf{w} \sim \mathcal{N}(0, \delta^{-1}\mathbf{I}_P)$. This completes the proof.

It is easy to see that the same proof works when using the approximations shown in (5). In that case, only the steps from (22) need to be modified. The proof also holds when a prior other than Gaussian and a model other than DNN is used. \square

A.2 Proof of Theorem 2

Similarly to the previous section, we start by writing the Gaussian approximation for VON. We will express its natural parameters in terms of the gradient and Hessians. A GGN approximation and some manipulation will show that the distributions found by VON correspond to posteriors of linear models.

The Gaussian approximation at the t 'th iteration of VON is denoted by $q_t(\mathbf{w}) := \mathcal{N}(\mathbf{w}|\boldsymbol{\mu}_t, \boldsymbol{\Sigma}_t)$ where $\boldsymbol{\Sigma}_t := (\mathbf{S}_t + \delta\mathbf{I}_P)^{-1}$ is obtained from \mathbf{S}_t . Using this, we can rewrite the updates (11) and (12) in terms of $\boldsymbol{\mu}_t$ and $\boldsymbol{\Sigma}_t^{-1}$ as follows

$$\boldsymbol{\mu}_{t+1} = \boldsymbol{\mu}_t - \beta_t \boldsymbol{\Sigma}_{t+1} \left[\sum_{i=1}^N \mathbb{E}_{q_t(w)} [\nabla_w \ell_i(\mathbf{w})] + \delta \boldsymbol{\mu}_t \right], \quad (24)$$

$$\boldsymbol{\Sigma}_{t+1}^{-1} = (1 - \beta_t) \boldsymbol{\Sigma}_t^{-1} + \beta_t \left[\sum_{i=1}^N \mathbb{E}_{q_t(w)} [\nabla_{ww}^2 \ell_i(\mathbf{w})] + \delta \mathbf{I}_P \right]. \quad (25)$$

It is again more convenient if we can have an update formula for the natural-parameters of the Gaussian distribution $\mathcal{N}(\mathbf{w}|\boldsymbol{\mu}_t, \boldsymbol{\Sigma}_t)$, denoted by $\boldsymbol{\eta}_t := \{\boldsymbol{\Sigma}_t^{-1} \boldsymbol{\mu}_t, -\frac{1}{2} \boldsymbol{\Sigma}_t^{-1}\}$. So we use similar techniques to find an update for $\boldsymbol{\eta}_t$. In addition, since there are no closed-form expressions for the expectations above, we use S number of samples $\mathbf{w}_t^{(s)} \sim q_t(\mathbf{w})$, for $s = 1, 2, \dots, S$, and use Monte Carlo (MC) approximation.

Given (25), the update corresponding to the second natural-parameter is obvious and given by

$$-\frac{1}{2} \boldsymbol{\Sigma}_{t+1}^{-1} = (1 - \beta_t) \left[-\frac{1}{2} \boldsymbol{\Sigma}_t^{-1} \right] - \frac{1}{2} \beta_t \left[\sum_{i=1}^N \mathbb{E}_{q_t(w)} [\nabla_{ww}^2 \ell_i(\mathbf{w})] + \delta \mathbf{I}_P \right] \quad (26)$$

$$\approx (1 - \beta_t) \left[-\frac{1}{2} \boldsymbol{\Sigma}_t^{-1} \right] - \frac{1}{2} \beta_t \left[\frac{1}{S} \sum_{i,s=1}^{N,S} \nabla_{ww}^2 \ell_i(\mathbf{w}_t^{(s)}) + \delta \mathbf{I}_P \right], \quad (27)$$

where we have used an MC approximation in the second step.

To write the update for the first natural-parameter, we multiply (24) by $\boldsymbol{\Sigma}_{t+1}^{-1}$ and get

$$\boldsymbol{\Sigma}_{t+1}^{-1} \boldsymbol{\mu}_{t+1} = \boldsymbol{\Sigma}_{t+1}^{-1} \boldsymbol{\mu}_t - \beta_t \left[\sum_{i=1}^N \mathbb{E}_{q_t(w)} [\nabla_w \ell_i(\mathbf{w})] + \delta \boldsymbol{\mu}_t \right] \quad (28)$$

$$= (1 - \beta_t) \left[\boldsymbol{\Sigma}_t^{-1} \boldsymbol{\mu}_t \right] + \beta_t \sum_{i=1}^N \left[-\mathbb{E}_{q_t(w)} [\nabla_w \ell_i(\mathbf{w})] + \mathbb{E}_{q_t(w)} [\nabla_{ww}^2 \ell_i(\mathbf{w})] \boldsymbol{\mu}_t \right] \quad (29)$$

$$\approx (1 - \beta_t) \left[\boldsymbol{\Sigma}_t^{-1} \boldsymbol{\mu}_t \right] + \frac{\beta_t}{S} \sum_{i,s=1}^{N,S} \left[-\nabla_w \ell_i(\mathbf{w}_t^{(s)}) + \nabla_{ww}^2 \ell_i(\mathbf{w}_t^{(s)}) \boldsymbol{\mu}_t \right], \quad (30)$$

where in the second step, we replaced $\boldsymbol{\Sigma}_{t+1}^{-1}$ in the first term by (25). The posterior approximation $q_{t+1}(\mathbf{w})$ at time $t + 1$ can be written in terms of natural parameters as shown below:

$$q_{t+1}(\mathbf{w}) = \frac{1}{\sqrt{(2\pi)^P |\boldsymbol{\Sigma}_{t+1}|}} \exp \left[-\frac{1}{2} (\mathbf{w} - \boldsymbol{\mu}_{t+1})^\top \boldsymbol{\Sigma}_{t+1}^{-1} (\mathbf{w} - \boldsymbol{\mu}_{t+1}) \right] \quad (31)$$

$$\propto \exp \left[-\frac{1}{2} \mathbf{w}^\top (\boldsymbol{\Sigma}_{t+1}^{-1}) \mathbf{w} + \mathbf{w}^\top (\boldsymbol{\Sigma}_{t+1}^{-1} \boldsymbol{\mu}_{t+1}) \right]. \quad (32)$$

By substituting the natural parameters from (27) and (30), we get the following update for $q_{t+1}(\mathbf{w})$, expressed in terms of the MC samples:

$$q_{t+1}(\mathbf{w}) \propto p(\mathbf{w})^{\beta_t} q_t(\mathbf{w})^{1-\beta_t} \times \prod_{i,s=1}^{N,S} \exp \left[-\frac{\beta_t}{2S} \mathbf{w}^\top \nabla_{\mathbf{w}\mathbf{w}}^2 \ell_i(\mathbf{w}_t^{(s)}) \mathbf{w} + \frac{\beta_t \mathbf{w}_t^\top}{S} \left\{ -\nabla_{\mathbf{w}} \ell_i(\mathbf{w}_t^{(s)}) + \nabla_{\mathbf{w}\mathbf{w}}^2 \ell_i(\mathbf{w}_t^{(s)}) \boldsymbol{\mu}_t \right\} \right], \quad (33)$$

where $p(\mathbf{w}) = \mathcal{N}(\mathbf{w}|0, \delta^{-1} \mathbf{I}_P)$ is the prior distribution. For the product of posterior approximation at time t and prior in (33), we obtain the following unnormalized Gaussian

$$p(\mathbf{w})^{\beta_t} q_t(\mathbf{w})^{1-\beta_t} = \mathcal{N}(\mathbf{w}|0, \delta^{-1} \mathbf{I}_P)^{\beta_t} \mathcal{N}(\mathbf{w}|\boldsymbol{\mu}_t, \boldsymbol{\Sigma}_t)^{1-\beta_t} \propto \mathcal{N}(\mathbf{w}|\mathbf{m}_t, \mathbf{V}_t), \quad (34)$$

where \mathbf{V}_t and \mathbf{m}_t are given by

$$\mathbf{V}_t^{-1} := (1 - \beta_t) \boldsymbol{\Sigma}_t^{-1} + \beta_t \delta \mathbf{I}_P, \quad \mathbf{m}_t := (1 - \beta) \mathbf{V}_t \boldsymbol{\Sigma}_t^{-1} \boldsymbol{\mu}_t. \quad (35)$$

Next, for the product over i and s in (33), we employ the GGN approximation (7) and get

$$\tilde{q}_{t+1}(\mathbf{w}) \propto \mathcal{N}(\mathbf{w}|\mathbf{m}_t, \mathbf{V}_t) \times \prod_{i,s=1}^{N,S} \exp \left[-\mathbf{w}^\top \mathbf{J}_{s,t}(\mathbf{x}_i)^\top \frac{\beta_t \boldsymbol{\Lambda}_{i,s,t}}{2S} \mathbf{J}_{s,t}(\mathbf{x}_i) \mathbf{w} + \frac{\beta_t \mathbf{w}^\top \mathbf{J}_{s,t}(\mathbf{x}_i)^\top}{S} \left\{ \boldsymbol{\Lambda}_{i,s,t} \mathbf{J}_{s,t}(\mathbf{x}_i) \boldsymbol{\mu}_t - \mathbf{r}_{i,s,t} \right\} \right], \quad (36)$$

where we have defined $\mathbf{J}_{s,t}(\mathbf{x}_i) := \mathbf{J}_{w_t^{(s)}}(\mathbf{x}_i)$, $\mathbf{r}_{i,s,t} := \mathbf{r}_{w_t^{(s)}}(\mathbf{x}_i, \mathbf{y}_i)$, and $\boldsymbol{\Lambda}_{i,s,t} := \boldsymbol{\Lambda}_{w_t^{(s)}}(\mathbf{x}_i, \mathbf{y}_i)$. The notation $\tilde{q}_{t+1}(\mathbf{w})$ is used to emphasize that GGN approximation is used in this update.

We are now ready to express each term in the product above as a Gaussian distribution. First, we define three quantities: $\mathbf{J}_t(\mathbf{x})$, $\mathbf{r}_t(\mathbf{x}, \mathbf{y})$ and $\boldsymbol{\Lambda}_t(\mathbf{x}, \mathbf{y})$ which are obtained by concatenating all the sampled Jacobians, residuals, and noise-precision matrices:

$$\mathbf{J}_t(\mathbf{x}) := \begin{bmatrix} \mathbf{J}_{w_t^{(1)}}(\mathbf{x}) \\ \mathbf{J}_{w_t^{(2)}}(\mathbf{x}) \\ \mathbf{J}_{w_t^{(3)}}(\mathbf{x}) \\ \vdots \\ \mathbf{J}_{w_t^{(S)}}(\mathbf{x}) \end{bmatrix}, \quad \mathbf{r}_t(\mathbf{x}, \mathbf{y}) := \begin{bmatrix} \mathbf{r}_{w_t^{(1)}}(\mathbf{x}, \mathbf{y}) \\ \mathbf{r}_{w_t^{(2)}}(\mathbf{x}, \mathbf{y}) \\ \mathbf{r}_{w_t^{(3)}}(\mathbf{x}, \mathbf{y}) \\ \vdots \\ \mathbf{r}_{w_t^{(S)}}(\mathbf{x}, \mathbf{y}) \end{bmatrix}, \quad (37)$$

$$\boldsymbol{\Lambda}_t(\mathbf{x}, \mathbf{y}) := \begin{bmatrix} \boldsymbol{\Lambda}_{w_t^{(1)}}(\mathbf{x}, \mathbf{y}) & 0 & 0 & \dots & 0 \\ 0 & \boldsymbol{\Lambda}_{w_t^{(2)}}(\mathbf{x}, \mathbf{y}) & 0 & \dots & 0 \\ 0 & 0 & \boldsymbol{\Lambda}_{w_t^{(3)}}(\mathbf{x}, \mathbf{y}) & \dots & 0 \\ \vdots & \vdots & \ddots & \vdots & \vdots \\ 0 & 0 & 0 & \dots & \boldsymbol{\Lambda}_{w_t^{(S)}}(\mathbf{x}, \mathbf{y}) \end{bmatrix}. \quad (38)$$

Using this, we define a transformed output of length $KS \times 1$ as

$$\tilde{\mathbf{y}}_{i,t} := \mathbf{J}_t(\mathbf{x}_i) \boldsymbol{\mu}_t - \boldsymbol{\Lambda}_t(\mathbf{x}_i, \mathbf{y}_i)^{-1} \mathbf{r}_t(\mathbf{x}_i, \mathbf{y}_i). \quad (39)$$

The distribution $\tilde{q}_{t+1}(\mathbf{w})$ defined in (36) can then be expressed as the following:

$$\tilde{q}_{t+1}(\mathbf{w}) \propto \mathcal{N}(\mathbf{w}|\mathbf{m}_t, \mathbf{V}_t) \prod_{i=1}^N \mathcal{N}(\tilde{\mathbf{y}}_{i,t} | \mathbf{J}_t(\mathbf{x}_i) \mathbf{w}, S(\beta_t \boldsymbol{\Lambda}_t(\mathbf{x}, \mathbf{y}))^{-1}). \quad (40)$$

As before, we can show that this distribution is equal to the posterior distribution of a linear on a transformed dataset defined as $\tilde{\mathcal{D}}_t := \{(\mathbf{x}_i, \tilde{\mathbf{y}}_{i,t})\}_{i=1}^N$. To model such outputs, we define a linear model for an output $\tilde{\mathbf{y}}_t \in \mathbb{R}^{KS}$ defined as follows:

$$\tilde{\mathbf{y}}_t = \mathbf{J}_t(\mathbf{x}) \mathbf{w} + \boldsymbol{\epsilon}_t, \quad \text{with } \boldsymbol{\epsilon}_t \sim \mathcal{N}(0, S(\beta_t \boldsymbol{\Lambda}_t(\mathbf{x}, \mathbf{y}))^{-1}), \quad \text{and } \mathbf{w} \sim \mathcal{N}(\mathbf{m}_t, \mathbf{V}_t). \quad (41)$$

The theorem presented in the main text is a simpler version of this theorem where $S = 1$. This completes the proof. \square

A.3 Linear Model Corresponding to OGGN

In OGGN, we evaluate the gradient and Hessian at the mean $\boldsymbol{\mu}_t$ defined to be equal to the current iterate \mathbf{w}_t . This corresponds to $S = 1$ in the setting described in the proof of theorem 2 (see Appendix A.2) with $\mathbf{w}_t^{(1)} := \mathbf{w}_t$. Therefore, the linear model is the same as before but with $\mathbf{J}_t(\mathbf{x})$, $\mathbf{r}_t(\mathbf{x}, \mathbf{y})$ and $\boldsymbol{\Lambda}_t(\mathbf{x}, \mathbf{y})$ defined at \mathbf{w}_t .

B Approximating Posterior Predictive with DNN2GP Approach

Typically, we can always predict using Monte Carlo sampling from the Gaussian approximation, however, this might be too noisy sometimes. In this section, we show how DNN2GP approach enables us to directly use the GP regression model for *approximating* the posterior predictive distribution. We elaborate on the method for Laplace approximation but this can be generalized to VI as briefly explained in subsection B.3.

Given a test input, denoted by \mathbf{x}_* , we first compute the feature map $\mathbf{J}_*(\mathbf{x}_*)^\top$. Using the linear model found in the DNN2GP approach, we can compute the posterior predictive distribution of the output, which we denote by $\tilde{\mathbf{y}}_*$. However, to be able to compute the predictive distribution for the true output \mathbf{y}_* , we need to *invert the map* from \mathbf{y}_* to $\tilde{\mathbf{y}}_*$. The expressions for this map can be obtained by using the definition of the transformed output $\tilde{\mathbf{y}}_* := \mathbf{J}_*(\mathbf{x}_*)\mathbf{w}_* - \boldsymbol{\Lambda}_*(\mathbf{x}_*, \mathbf{y}_*)^{-1}\mathbf{r}_*(\mathbf{x}_*, \mathbf{y}_*)$. We demonstrate this for two common cases of squared loss and logistic loss.

B.1 Laplace Approximation and Squared Loss

Consider the squared loss, $\ell(\mathbf{y}, \mathbf{f}_w(\mathbf{x})) = \frac{1}{2\sigma^2}\|\mathbf{y} - \mathbf{f}_w(\mathbf{x})\|^2$ with σ^2 as the noise variance. According to section 3, in this case, we have $\mathbf{r}_*(\mathbf{x}, \mathbf{y}) := \sigma^{-2}(\mathbf{f}_{w_*}(\mathbf{x}) - \mathbf{y})$ and $\boldsymbol{\Lambda}_*(\mathbf{x}, \mathbf{y}) := \sigma^{-2}\mathbf{I}_K$. Using these expressions in the definition for $\tilde{\mathbf{y}} := \mathbf{J}_*(\mathbf{x})\mathbf{w}_* - \boldsymbol{\Lambda}_*(\mathbf{x}, \mathbf{y})^{-1}\mathbf{r}_*(\mathbf{x}, \mathbf{y})$, we get the following map for the test input \mathbf{x}_* :

$$\tilde{\mathbf{y}}_* = \mathbf{J}_*(\mathbf{x}_*)\mathbf{w}_* - (\mathbf{f}_{w_*}(\mathbf{x}_*) - \mathbf{y}_*) \quad (42)$$

$$\implies \mathbf{y}_* = \tilde{\mathbf{y}}_* + \mathbf{f}_{w_*}(\mathbf{x}_*) - \mathbf{J}_*(\mathbf{x}_*)\mathbf{w}_* \quad (43)$$

Given a predictive distribution for $\tilde{\mathbf{y}}_*$ computed by the linear model (8) with the posterior distribution $\mathcal{N}(\mathbf{w}|\mathbf{w}_*, \tilde{\boldsymbol{\Sigma}})$, we can therefore derive the predictive distribution for \mathbf{y}_* . In the example above, the predictive variance of $\tilde{\mathbf{y}}_*$ and \mathbf{y}_* will be the same, while the predictive mean of \mathbf{y}_* is obtained by adding $\mathbf{f}_{w_*}(\mathbf{x}_*) - \mathbf{J}_*(\mathbf{x}_*)\mathbf{w}_*$ to the mean of $\tilde{\mathbf{y}}_*$. The result is as follows

$$\mathbf{y}_*|\mathbf{x}_*, \mathcal{D} \sim \mathcal{N}\left(\mathbf{y}_*|\mathbf{f}_{w_*}(\mathbf{x}_*), \mathbf{J}_*(\mathbf{x}_*)\tilde{\boldsymbol{\Sigma}}\mathbf{J}_*(\mathbf{x}_*)^\top + \sigma^2\mathbf{I}_K\right). \quad (44)$$

We use this technique to compute the predictive distribution in Fig. 3 (labeled as ‘DNN2GP’ in the plots).

B.2 Laplace Approximation and Logistic Loss

The procedure above for *inversion of maps* generalizes to other loss functions derived using generalized linear models. We need to assume that the loss corresponds to a log probability distribution, i.e., $\ell(\mathbf{y}, \mathbf{f}_w(\mathbf{x})) := -\log p(\mathbf{y}|\mathbf{h}(\mathbf{f}_w(\mathbf{x})))$ where $\mathbf{h}(\cdot)$ is a *link function*. We now describe this for a Bernoulli distribution $y_i \in \{0, 1\}$ using the results in section 3.

Similarly to the squared-loss case, we need to write $\tilde{\mathbf{y}}$ in terms of the true output \mathbf{y} . For a Bernoulli likelihood, the link function is $\sigma(\mathbf{f}_{w_*}(\mathbf{x})) := p_*(\mathbf{x})$ where σ is the sigmoid function, the residual is $\mathbf{r}_*(\mathbf{x}, \mathbf{y}) = p_*(\mathbf{x}) - \mathbf{y}$, and the noise precision is $\boldsymbol{\Lambda}_{w_*}(\mathbf{x}, \mathbf{y}) = p_*(\mathbf{x})(1 - p_*(\mathbf{x})) := \boldsymbol{\lambda}_*(\mathbf{x})$. We again use the definition for the transformed output and write the map for the test input \mathbf{x}_* :

$$\tilde{\mathbf{y}}_* = \mathbf{J}_*(\mathbf{x}_*)\mathbf{w}_* - \boldsymbol{\lambda}_*(\mathbf{x}_*)^{-1}(p_*(\mathbf{x}_*) - \mathbf{y}_*) \quad (45)$$

$$\implies \mathbf{y}_* = p_*(\mathbf{x}_*) + \boldsymbol{\lambda}_*(\mathbf{x}_*)\tilde{\mathbf{y}}_* - \boldsymbol{\lambda}_*(\mathbf{x}_*)\mathbf{J}_*(\mathbf{x}_*)\mathbf{w}_* \quad (46)$$

Given the predictive distribution over $\tilde{\mathbf{y}}_*$ at the test input \mathbf{x}_* , we can then compute the corresponding distribution over \mathbf{y}_* . The predictive distribution of $\tilde{\mathbf{y}}_*$ in the linear model (8) with the posterior distribution $\mathcal{N}(\mathbf{w}|\mathbf{w}_*, \tilde{\boldsymbol{\Sigma}})$ is given as follows:

$$\tilde{\mathbf{y}}_*|\mathbf{x}_*, \tilde{\mathcal{D}} \sim \mathcal{N}\left(\tilde{\mathbf{y}}_*|\mathbf{J}_*(\mathbf{x}_*)\mathbf{w}_*, \boldsymbol{\lambda}_*(\mathbf{x}_*)^{-1} + \mathbf{J}_*(\mathbf{x}_*)\tilde{\boldsymbol{\Sigma}}\mathbf{J}_*(\mathbf{x}_*)^\top\right). \quad (47)$$

Therefore, using the map (46), we get the following predictive distribution over y_* :

$$y_* | \mathbf{x}_*, \mathcal{D} \sim \mathcal{N} \left(y_* | \sigma(f_{w_*}(\mathbf{x}_*)), \lambda_*(\mathbf{x}_*) + \lambda_*(\mathbf{x}_*)^2 \mathbf{J}_*(\mathbf{x}_*) \tilde{\Sigma} \mathbf{J}_*(\mathbf{x}_*)^\top \right). \quad (48)$$

Similar to the linear basis function model, the two terms in the predictive variance have an interpretation (e.g., see [1] Eq. 3.59). The first term can be interpreted as the aleatoric uncertainty (label noise), while the second term takes a form that resembles the epistemic uncertainty (model noise). Such interpretation is possible due to the conversion of a DNN to a linear-basis function model in our DNN2GP framework.

This approach can be similarly written for other Gaussian approximations. It can also be generalized to loss functions obtained using the generalized linear model. The inversion of the map is possible whenever the link function $\mathbf{h}(\cdot)$ is invertible.

B.3 Generalization to VI

For the VOGGN update with one MC sample, we can use the same procedure as above. The same is true for OGGN since one MC sample is replaced by the mean. For VOGGN with multiple MC samples, we get S such maps. Each of those maps give us a prediction, denote it by $\tilde{y}_{*,s,t}$ for sample s at iteration t . To obtain the final prediction, we can use the average all predictions $\tilde{y}_{*,s,t}$ over $s = 1, 2, 3, \dots, S$ to get the predictive distribution for $\mathbf{y}_{*,t}$.

C Additional Results

In this appendix, we provide additional figures to the ones presented in Sec. 5.2.

C.1 Further Posteriors and Kernels for MNIST and CIFAR

Fig. 7 is similar to Fig. 4a but uses the variational approximation instead of a Laplace approximation. While the posterior mean on MNIST shows very similar structure for both approximations, the kernel shows some interesting differences. There are many more negative correlations between examples from different classes in the kernel corresponding to the variational approximation. The posterior mean on CIFAR-10 has similar structure yet it appears to exhibit higher uncertainty. In Fig. 8, we show the kernel matrix on 300 data points of CIFAR-10 with the respective class labels. The kernel is computed for both the Laplace and variational approximation but shows less structure than that of the MNIST dataset.

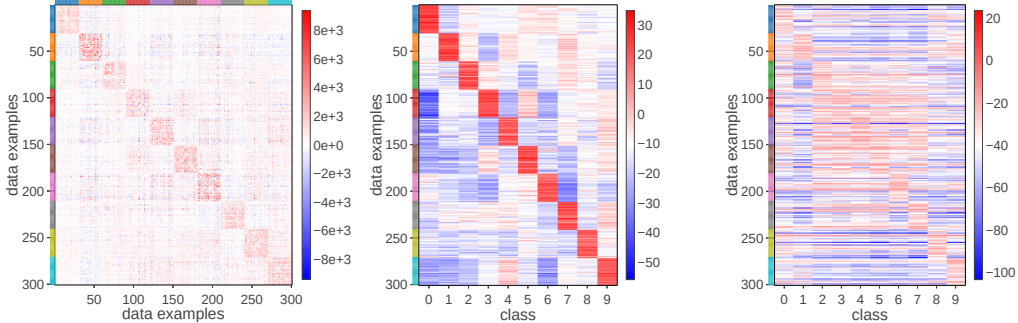


Figure 7: This figure visualizes the GP kernel matrix and posterior mean for LeNet5 trained with VOGN on MNIST (left) and CIFAR-10 (right). The kernel matrix clearly shows the correlations learned by the DNN. A higher posterior mean is assigned to the correct label which reflects the accuracy obtained by the DNN.

C.2 Uncertainties according to DNN2GP for Classification

In this section we present a toy example for the classification task in line with the regression experiment in Fig. 3. We use the reparameterization introduced in App. B.2, in particular Eq. (48).

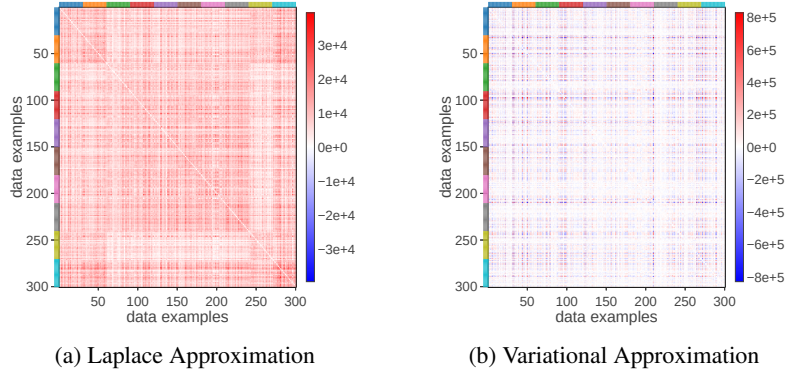


Figure 8: GP kernels due to Laplace and variational approximation for neural networks on CIFAR-10. The kernels show slight traces of structure but are not as significant as the ones presented on MNIST in Sec. 5.

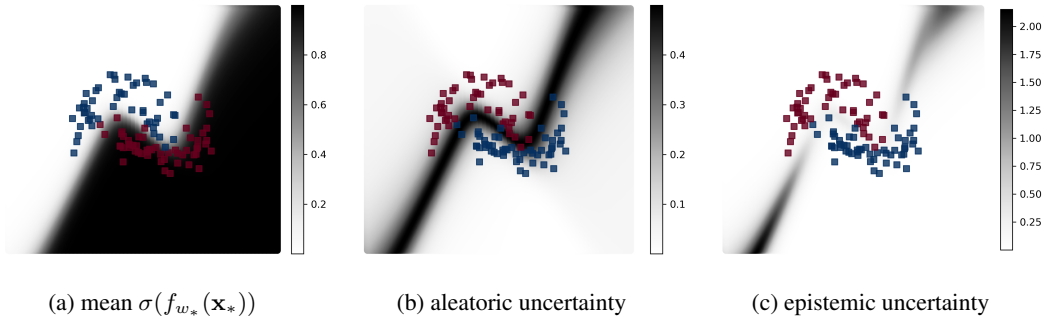


Figure 9: This figure demonstrates the decomposition of predictive variances due to the reparameterization introduced in App. B.2 on a binary toy classification task (red vs. blue half moons). We plot the quantities of Eq. (48) in figures (a)-(c): (a) is the prediction of a trained NN while the sum of (b) and (c) give us the posterior predictive uncertainties. Around the decision boundary, the label noise (b) is high and remains unchanged further from the data while the predictive uncertainty is low where supported by data and strongly grows away from it. Here, the model fits the data well in contrast to Fig. 4d where the model is unable to do so which results in high estimated label noise.

We train a neural network with single hidden layer of 10 units and tanh activation to fit the non-linear decision boundary. We have $\delta = 0.26$ and train on 100 samples for 5000 full-batch epochs. Fig. 9 shows how the reparameterization allows to decompose predictive variance into label noise due to the decision boundary, see. (b), and model uncertainty, see (c), that grows away from the data.

D Author Contributions Statement

Author List: Mohammad Emtiyaz Khan, Alexander Immer, Ehsan Abedi, Maciej Kozzepa.

M.E.K. conceived a rough idea using the gradients and Hessians of the loss, and wrote the first version of the proofs. A.I. and E.A. made major corrections to M.E.K.’s original version and introduced version used in the final paper. They also came up with the prediction method for DNN2GP. E.A. formalized the NTK connection, and extensively studied its connection to the GP posterior. A.I. did most of the experiments and introduced the necessary reparameterization for applications. M.K. helped on the hyperparameter-tuning experiments, as well as with the visualizations. M.K. did the regression uncertainty experiment with some help from E.A. and A.I.

M.E.K. wrote the main content of the paper. E.A. wrote all the proofs, and A.I. and M.K. summarized the experiment section. All the authors proof-read the paper and revised it.

E Camera-Ready Version vs the Submitted Version

We made several changes taking reviewers feedback into account.

1. The writing and organization of the papers were modified to emphasize that we are able to relate the iterations of a deep-learning algorithm to GP inference.
2. To improve clarity, Fig. 1 was added as a summary of our approach. The writing was modified to follow Step A, B, and C given in Fig. 1.
3. Titles of Section 3 and 4 were changed to emphasize relationship to "solutions and iterations" of a deep-learning algorithm.
4. Theorem 1 and 2 were simplified to focus only on the posterior of linear model only. Relation to GP is discussed separately.
5. Experiment on GP regression was modified to focus on uncertainty instead of the width of the DNN.
6. Visualization of the GP predictive uncertainty and noise was added on top of predictive mean on CIFAR-10
7. A real-world experiment on Wine dataset was added, where we tune the width of the DNN.